How to cite: Angew. Chem. Int. Ed. 2024, e202416549
doi.org/10.1002/anie.202416549

Ion Channels

Optical Control of TRPM8 Channels with Photoswitchable Menthol

Jasmin Becker[+], Clara S. Ellerkmann[+], Hannah Schmelzer[+], Christian Hermann, Kyra Lützel, Thomas Gudermann, David B. Konrad, Dirk Trauner,* Ursula Storch,* and Michael Mederos y Schnitzler**

Abstract: Transient receptor potential melastatin 8 (TRPM8) channels are well known as sensors for cold temperatures and cooling agents such as menthol and icilin and these channels are tightly regulated by the membrane lipid phosphoinositol-4,5-bisphosphate (PIP_2). Since TRPM8 channels emerged as promising drug targets for treating pain, itching, obesity, cancer, dry eye disease, and inflammation, we aimed at developing a high-precision TRPM8 channel activator, to achieve spatiotemporal control of TRPM8 activity with light. In this study, we designed, synthesized and characterized the first photoswitchable TRPM8 activator azo-menthol (AzoM). AzoM enables optical control of endogenously and heterologously expressed TRPM8 channels with UV and blue light which is demonstrated by performing patch-clamp experiments. Moreover, AzoM facilitates the reliable determination of activation, inactivation, and deactivation kinetics thereby providing further insights into the channel gating. Using AzoM, the specific roles of individual amino acids for AzoM or PIP_2 binding and for sensitization by PIP_2 can be elucidated. Altogether, AzoM represents as a high-precision pharmaceutical tool for reversible control of TRPM8 channel function that enhances our biophysical understanding of TRPM8 channels and holds the potential to support the development of novel pharmaceuticals.

Introduction

Transient receptor potential melastatin 8 (TRPM8) channels belong to the transient receptor potential (TRP) channel superfamily. TRPM8 channels are non-selective cation channels that act as cold sensors in the somatosensory system[1] and are well known as sensors for the natural cooling agent menthol[2] as well as for synthetic cooling agents such as icilin.[3] The importance of TRPM8 (and of the heat and pain sensor TRPV1) is underscored by the awarding of the Nobel Prize to David Julius in 2021 for their discovery.

Several physiological and pathophysiological roles of TRPM8 channels haven been identified so far. TRPM8 channels are expressed in unmyelinated C fibers which are peripheral sensory neurons of small size that sense and transduce cold stimuli,[2,4] and are found in various other tissues like prostate, bladder, urogenital tract, cardiovascular and bronchopulmonary tissue.[5] Notably, the loss of TRPM8 expression in TRPM8 gene-deficient mice is not only correlated to an impaired cold but also to an impaired warm sensation[6] suggesting a pivotal role of TRPM8 for temperature sensing and thermoregulation. Moreover, TRPM8 is involved in various pathophysiological states, such as in pain

[*] J. Becker,[+] C. S. Ellerkmann,[+] H. Schmelzer,[+] C. Hermann, Prof. Dr. T. Gudermann, Prof. Dr. U. Storch, Prof. Dr. M. Mederos y Schnitzler
Walther Straub Institute of Pharmacology and Toxicology
Ludwig Maximilian University of Munich
Goethestr. 33, 80336 Munich, Germany
E-mail: mederos@lrz.uni-muenchen.de

Prof. Dr. U. Storch
Institute of Pharmacy
University of Regensburg
Universitätsstr. 31, 93040 Regensburg, Germany
E-mail: ursula.storch@chemie.uni-regensburg.de

Prof. Dr. D. Trauner
Department of Chemistry
College of Arts and Sciences
University of Pennsylvania
231 South 34th Street, Philadelphia, Pennsylvania 19104-6323, United States
E-mail: dtrauner@upenn.edu

K. Lützel, Dr. D. B. Konrad
Department of Pharmacy
Ludwig Maximilian University of Munich
Butenandtstr. 5–13, 81377 Munich, Germany
E-mail: david.konrad@cup.lmu.de

Prof. Dr. T. Gudermann
Comprehensive Pneumology Center Munich (CPC–M)
German Center for Lung Research
81377 Munich, Germany

Prof. Dr. T. Gudermann, Prof. Dr. M. Mederos y Schnitzler
DZHK (German Centre for Cardiovascular Research)
Munich Heart Alliance
80336 Munich, Germany

[+] These authors contributed equally to this work

sensation. A reduced TRPM8 expression is correlated with a reduced migraine risk and with a decreased sensation of cold-induced pain.[7] However, a hypersensitivity of TRPM8 leads to cold allodynia during pathological conditions such as inflammation or nerve injury.[8] Furthermore, alterations in expression of TRPM8 is related to different kinds of cancer including prostate, pancreas, breast, lung, skin and colon cancer.[9] TRPM8 expression is also linked to dry eye disease,[10] overactive bladder, irritable bowel syndrome, oropharyngeal dysphagia, chronic cough and hypertension.[11] In addition, TRPM8 plays a role for obesity and type 2 diabetes.[12] Thus, TRPM8 channels emerged as promising drug targets for various pathophysiological conditions, highlighting the need for potent TRPM8 modulators that could serve as novel treatments for TRPM8-related diseases. To develop precise channel modulators with specific modes of action, detailed knowledge of the channel's regulation and ligand-binding mechanisms is essential.

Recent advances in structural analysis using cryo-electron microscopy (cryo-EM) have provided insights into the binding sites for synthetic TRPM8 channel activators such as icilin, WS-12,[13] 1-disopropylphosphorylnonate (C3)[14] or allyl isothio-cyanate (AITC).[15] However, structural analysis of a TRPM8 channel in the presence of (−)-menthol is still lacking. Furthermore, it is well known, that TRPM8 activity largely depends on the presence of the membrane phospholipid phosphatidylinositol 4,5-bisphosphate (PIP_2). By analyzing reconstituted TRPM8 channels in planar lipid bilayers it was shown that TRPM8 is functional only in the presence of PIP_2[16] and that PIP_2 binding sensitizes TRPM8 towards stimulation with cold temperature or cooling agents.[16]

To further decipher the role of TRPM8 in health and disease, we aimed at developing a novel photoswitchable TRPM8 channel activator based on the natural cooling agent menthol that can be switched ON and OFF with the spatiotemporal precision of light.

Photoswitching is commonly achieved by incorporating a photoswitchable azobenzene moiety, which enables *cis-trans* isomerization through UV or blue light. Advances in photopharmacology have already led to the development of several high-precision pharmaceutical tools, allowing for spatiotemporal control of protein function simply by switching light.[17]

A variety of photoswitchable TRP channel ligands that target TRPC[18,19,20],TRPV1[21,22] or TRPA1[23] channels have been developed so far. These photopharmaceuticals offer an additional advantage due to their rapid transition times from the *trans* to the *cis* configuration, occurring within a two-digit picosecond range, making them highly suitable for determining the activation and deactivation kinetics of currents.[24]

In this study, we designed, synthesized and characterized the photoswitchable menthol derivative azo-menthol (AzoM) demonstrating its ability to reversibly control TRPM8 channel activity via light. AzoM allows precise determination of activation and deactivation kinetics without the wash-in and wash-out effects typically seen with bath-applied ligands. By examining changes in current kinetics in AzoM and PIP_2 binding mutants, we identified and characterized potential binding sites. Additionally, we analyzed the influence of PIP_2 on current kinetics and discovered a PIP_2 sensitization mutant. Overall, AzoM provides valuable insights into the regulation of TRPM8 channel activity.

Results and Discussion

Synthesis and Characterization of Photoswitchable Azo-Menthol

To allow for a precise and optical control over TRPM8 channels we developed a photoswitchable menthol-derived chemical probe. Hereby, an optical switch is incorporated via azologization of the backstrategy that entails the replacement of a chemical fragment within a pharmacophore that is structurally related to azobenzene with this chemical photoswitch.[18,21a,25] (−)-Menthol is a known TRPM8 channel activator with an EC_{50} of 200 μM while CPS-125 exhibited an EC_{50} of 32 μM in the same study.[26] However, the EC_{50} values for (−)-menthol vary strongly between 4 and 200 μM in literature.[2a,26–27] We based our azologization strategy on the hypothesis that the biaryl sulfonylamide group in CPS-125[26] serves as a *cis*-azoster and could therefore be substituted for an azobenzene moiety without significant loss of bioactivity. To synthesize azo-menthol (AzoM) (Figure 1A), menthol carboxylic acid (**1**) was first prepared through a literature procedure.[28] The menthol carboxylic acid (**1**) was then converted to menthol carboxylic acid chloride (**2**) with oxalyl chloride and coupled with 4-aminoazobenzene (**3**) to give AzoM (Supplemental Figure 1).

AzoM allowed for *cis* and *trans* isomerization by applying blue light or UV light, respectively (Figure 1B). For detailed characterization of AzoM, we determined the photostationary states (PSS), the reversibility of photoswitching and the thermal relaxation. The PSS, which is the equilibrium state between the *trans* and *cis* configuration at a given illumination wavelength, was first estimated using UV/Vis spectroscopy (Figure 1C). The maximal absorption peak of *trans*-AzoM was at 359 nm and of *cis*-AzoM at 439 nm. The proportion of the *cis* isomer can be semi-quantitatively determined.[29] In the dark, after complete thermal relaxation, 100 % of the *trans* configuration was achieved. In order to obtain a PSS with the highest percentage of the *trans* configuration the most appropriate illumination wavelength was 525 nm resulting in 84 % *trans* and 16 % *cis* configuration. Focusing on the illumination wavelength of 435 nm, which is closest to the wavelength used in patch-clamp measurements to induce the *trans* configuration, we found that AzoM achieves approximately 78 % *trans* and 22 % *cis* configuration. The illumination with 365 nm resulted in 15 % *trans* and 85 % *cis* configuration. For a more precise quantitative analysis of the PSS, we used ^{1}H NMR spectroscopy (Supplemental Figure 2). The dark-adapted compound was measured after thermal relaxation

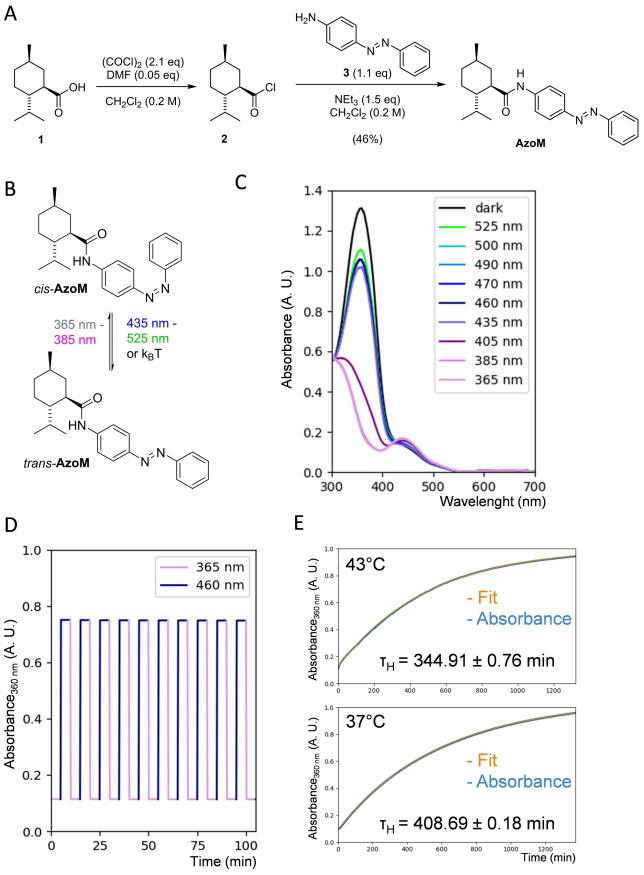

Figure 1. Synthesis and characterization of photoswitchable azo-menthol. (A) Synthesis of azo-menthol (AzoM) using menthol carboxylic acid (1) that was converted to menthol carboxylic acid chloride (2) with oxalyl chloride and coupled with 4-aminoazobenzene (3) to give AzoM. (B) Chemical structures of AzoM in its *cis* and *trans* configuration (*cis*-azo-menthol; *cis*-AzoM and *trans*-azo-menthol; *trans*-AzoM). (C) UV/Vis spectroscopic analysis of AzoM. Spectral absorbance from 300 nm to 700 nm was measured at 22 °C. The dark-adapted compound was measured after thermal relaxation for 3 days at 70 °C. (D) UV/Vis spectroscopic analysis of AzoM. Absorbance was measured at 360 nm at 22 °C. Compound was repeatedly illuminated with 365 nm and 460 nm light for 5 minutes each over a period of 110 minutes. (E) UV/Vis spectroscopy of AzoM. The compounds were pre-illuminated with 365 nm followed by relaxation in the dark at 43 °C and at 37 °C. The thermal relaxation was determined through UV/Vis analysis by measuring the time-dependent absorption at 360 nm with $A(t) = A_0 \cdot e^{\frac{-\ln(2) \cdot t}{\tau_H}} + c$. A_0: initial absorbance; c: maximal absorbance; τ_H: of half-life time constant. Fitted curve in orange and measured absorbance in blue. (C–E) UV/Vis spectroscopy was done with 50 µM AzoM in 9:1 $(CD_3)_2SO$:D_2O.

for 3 days at 70 °C leading to full *trans* configuration (100 % *trans* and 0 % *cis* configuration). Illumination of AzoM with 435 nm resulted in a ratio of 69 % *trans* and 31 % *cis* configuration, and illumination with 365 nm caused a ratio of 5 % *trans* and 95 % *cis* configuration.

To analyze the reversibility of photoswitching using UV/Vis spectroscopy, AzoM was repeatedly illuminated with alternating wavelengths of 365 nm and 460 nm for a total time of 110 minutes at 22 °C (Figure 1D). Within this period of time no changes in maximal and minimal absorptions were observed suggesting that photoswitching is fully reversible and that the compound does not degrade.

Furthermore, we analyzed the thermal relaxation rate using UV/Vis-spectroscopy. This property refers to the thermal transition from the *cis* to the *trans* configuration in the dark after application of 365 nm light. The half-life time constant (τ_H) for thermal relaxation was 344.91 ± 0.76 minutes at 43 °C and 408.09 ± 0.18 minutes at 37 °C (Figure 1E), suggesting that complete relaxation from the *cis* to the *trans* configuration occurs after approximately 29 hours at 43 °C or 34 hours at 37 °C (50 µM solution in 9:1 $(CD_3)_2SO$:D_2O).

Optical Control of TRPM8 with AzoM

To ascertain the suitability of AzoM for optical control over TRPM8 channel activity, we performed patch-clamp measurements in the whole-cell configuration with HEK293T cells overexpressing TRPM8 in the presence of 200 µM AzoM which is equimolar to the maximally effective concentration of the TRPM8 activator (−)-menthol utilized in our experiments. Switching to UV light or blue light that establishes the active *cis* (*cis*-AzoM) or the inactive *trans* (*trans*-AzoM) configuration caused TRPM8 current density (CD) increases or decreases at room temperature (Figure 2A–2C). Since TRPM8 channels are cold sensors that are strongly temperature dependent and have a temperature coefficient Q_{10} of about 24 at temperatures between 18 and 25 °C,[30] TRPM8 was already activated at room temperature. To suppress these cold-induced currents, the measurements were repeated at 37 °C which resulted in largely reduced CD amplitudes (Figure 2D–2F). However, *cis*-AzoM was effective at both temperatures and elicited significant TRPM8 CD increases. In the absence of AzoM, no CD changes were detected by light switching neither at room temperature or at 37 °C (Figures 2A, 2D and 2G). The summary of the maximal *trans*- and *cis*-AzoM-induced CD in outward and inward direction at ±100 mV (Figure 2B and 2E) shows significant CD increases in the presence of *cis*-AzoM compared to *trans*-AzoM with characteristic current density voltage (CDV) relationships (Figure 2C and 2F) indicating that AzoM is appropriate for optical control of TRPM8 channels. Interestingly, at 37 °C, when cold-induced currents are largely diminished, the *trans*-AzoM-induced CD at +100 mV are significantly reduced compared to the basal CD in the absence of AzoM (Figure 2E). Application of increasing concentrations of *trans*-AzoM at room temperature resulted in stepwise reductions of the cold-induced TRPM8 currents (Figure 2I) suggesting that *trans*-AzoM has a concentration-dependent inhibitory effect with an estimated IC_{50} of about 103 µM. These findings indicate that *trans*-AzoM is already bound in the binding pocket of the TRPM8 channel.

The EC_{50} value for *cis*-AzoM at 37 °C was estimated at 4.4 ± 5.8 µM with a slope of 0.5 ± 0.3 (Figure 2H). Thus, 50 µM AzoM represent the maximally effective concentration and was therefore used in all further experiments.

As a control, the TRPM8 activators (−)-menthol (200 µM) and icilin (10 µM) were applied in their maximally

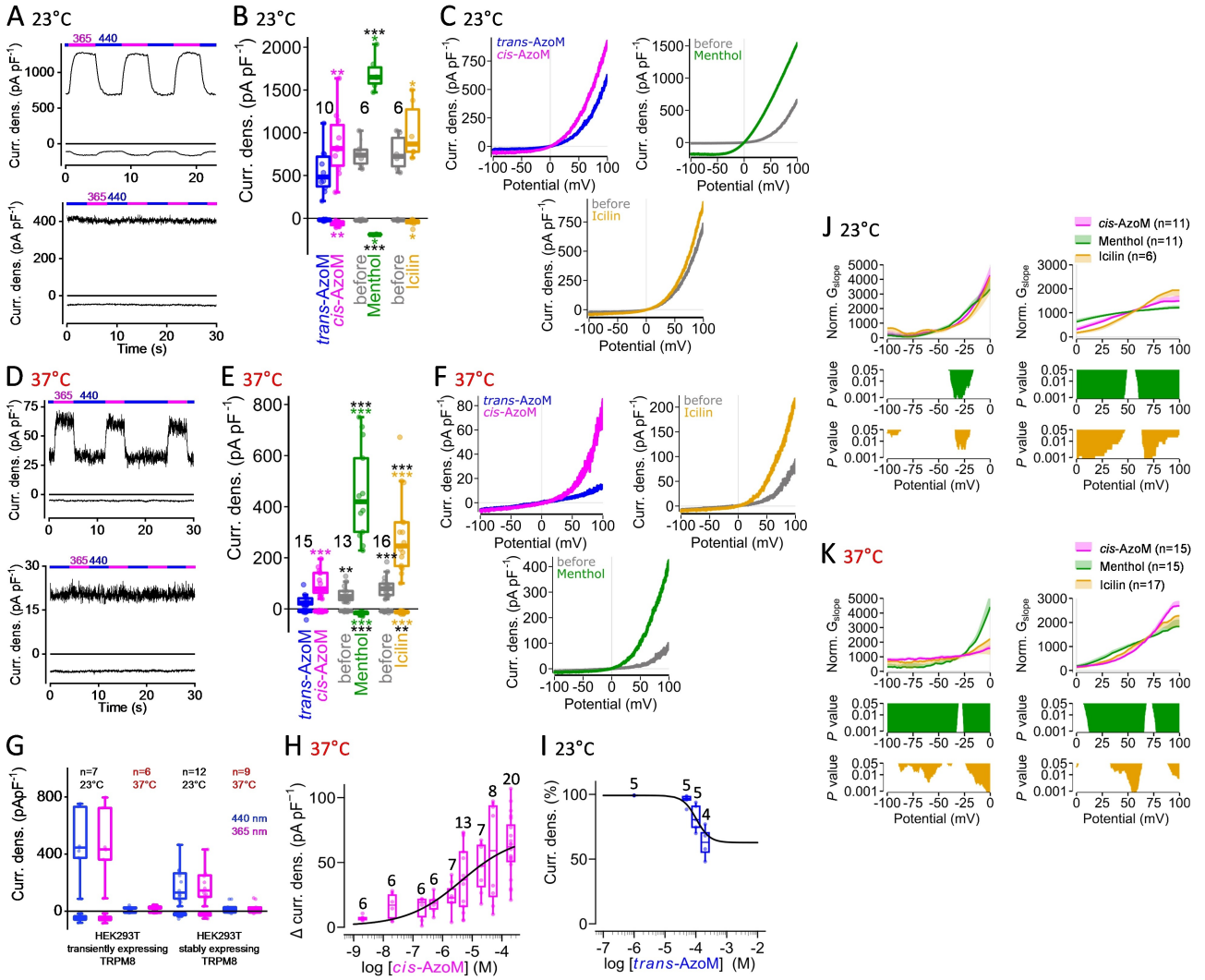

Figure 2. Optical control of TRPM8 with azo-menthol (AzoM). Whole-cell measurements of TRPM8 overexpressing HEK293T cells. (A, D) Representative current density (CD) time courses at ±100 mV in the presence (above) or absence (below) of AzoM (200 µM) measured at 23 °C (A) and 37 °C (D). Illumination with UV light (λ = 365 nm) and blue light (λ = 440 nm) is indicated. (B, E, G) Summaries of maximal CD ('Curr. dens.') at potentials of ±100 mV at 23 °C (B, G) and 37 °C (E, G) in the presence (B, E) or absence (G) of AzoM. (C, F) Representative CD voltage (CDV) relations in the presence of 200 µM *trans*- (*trans*-AzoM) and *cis*-azo-menthol (*cis*-AzoM) and before and during application of 200 µM (−)-menthol and 10 µM icilin. Numbers over boxplots indicate number of measured cells. Black asterisks indicate significance compared to *trans*- or *cis*-AzoM (***$P < 0.001$, **$P < 0.01$; Mann-Whitney U test), colored asterisks indicate significances between *trans*- and *cis*-AzoM, or between menthol- or icilin-induced CD compared to basal CD in the absence of the activators (**$P < 0.01$, ***$P < 0.001$; Wilcoxon matched-pairs signed-rank test). (H) Concentration response curve to determine EC_{50} of *cis*-AzoM at 37 °C with HEK293T cells stably expressing TRPM8. (I) Concentration response curve of cold-induced TRPM8 currents at 23 °C before and during application of increasing concentrations of *trans*-AzoM. (J, K) The normalized slope conductance (NSC) ('Norm. G_{slope}') of the CDV curves which was separately calculated for inward and outward currents (left and right graphs). The NSC is displayed as mean ± SD. *P* values are calculated using Mann-Whitney U test compared to *cis*-AzoM-induced NSC. (B, E, G, H, I) Data are displayed as boxplots and interquartile ranges. A slow up-ramp protocol with a frequency of 2 Hz was applied.

effective concentrations. (−)-menthol elicited significantly higher CD increases compared to *cis*-AzoM (Figure 2B and 2E) at 23 °C and 37 °C. The icilin-induced CD were significantly higher than the *cis*-AzoM-induced CD only at 37 °C (Figure 2E) suggesting that icilin is more effective when cold-induced TRPM8 currents are diminished. However, the icilin-induced CD increases were lower than the (−)-menthol-induced CD (Figure 2B and 2E).

To investigate differences between the CDV curves elicited by the TRPM8 channel activators *cis*-AzoM, (−)-menthol and icilin, we calculated the normalized slope conductance (NSC), which is a tool for a quantitative in-depth analysis of CDV curves. At 23 °C, the slope progressions of *cis*-AzoM-, (−)-menthol- and icilin-induced NSC curves mainly differs at positive potentials. At negative potentials, the NSC only slightly differs in the range of −40 to −20 mV (Figure 2J). At positive potentials, the curve progression of the NSC of *cis*-AzoM lies in between the two other NSC curves (Figure 2J) suggesting an intermediate channel state. At 37 °C, the NSC progression of the (−)-

menthol-induced current strongly differs from the NSC of the *cis*-AzoM- or the icilin-induced currents (Figure 2K) in particular at negative potentials, where the icilin- and *cis*-AzoM-induced NSC are more similar in their curve progressions. However, at positive potentials, the NSC of the icilin- and (−)-menthol-induced currents are more alike in their curve progression and strongly differ from the NSC of *cis*-azoM indicating that *cis*-AzoM elicits a distinct active channel state. Comparing the NSC of the basal TRPM8 currents before application of icilin or (−)-menthol with the NSC in the presence of *trans*-AzoM shows only minor differences at room temperature (Supplemental Figure 3). However, at 37 °C, the NSC of the *trans*-AzoM-induced current is significantly different to the NSC of the basal currents in the absence of any activators (Supplemental Figure 3) corroborating the finding that *trans*-AzoM has an inhibitory effect on TRPM8. Altogether, *trans*- and *cis*-AzoM elicit distinct NSC curves that are different from the icilin- or (−)-menthol-induced NSC curves suggesting that all three TRPM8 channel activators cause distinct active channel states. In addition, the NSC analysis allowed for determination of a distinct *trans*-AzoM induced inactive channel state.

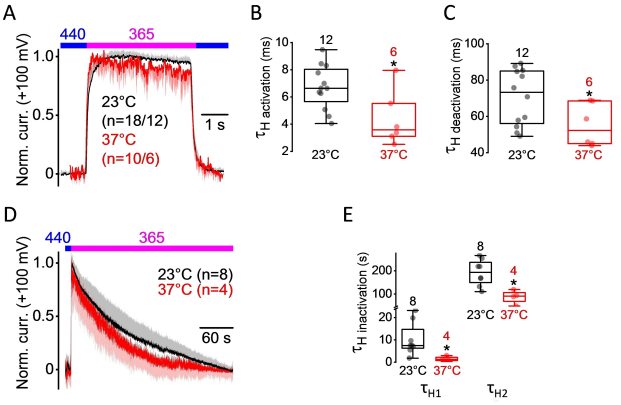

Figure 3. Activation, inactivation and deactivation kinetics of TRPM8 currents. Whole-cell measurements of TRPM8 overexpressing HEK293 cells in the presence of 50 µM AzoM. (A) Normalized current time courses at +100 mV determined by application of a fast up-ramp protocol with a frequency of 50 Hz measured at 23 °C and 37 °C displayed as median ± SD. Illumination with 440 and 365 nm is indicated. (B, C) Summaries of the half-time constants for activation (B, $\tau_{H\ activation}$) and inactivation (C, $\tau_{H\ deactivation}$) at 23 °C (black) and at 37 °C (red). Asterisks indicate significance compared to 23 °C (*$P<0.05$, Mann-Whitney U test). (D) Normalized current time courses at +100 mV determined by application of a fast up-ramp protocol with a frequency of 50 Hz measured at 23 °C and 37 °C with constant illumination with 365 nm. (E) Summaries of the half-time constants for fast (τ_{H1}) and slow inactivation (τ_{H2}) at 23 °C (black) and at 37 °C (red). Asterisks indicate significance compared to 23 °C (*$P<0.05$, Mann-Whitney U test). (B, C, E) Numbers over boxplots indicate number of measured cells. Data are displayed as boxplots and interquartile ranges. (A, D) Illumination protocol using light of the wavelengths $\lambda=365$ nm or $\lambda=440$ nm is depicted above the traces.

Activation, Deactivation and Inactivation Kinetics of TRPM8 Currents

To find out whether AzoM is suitable to precisely determine the activation and deactivation kinetics of TRPM8 currents without disturbing wash-in and wash-out effects that usually occur when using perfusion systems, we analyzed the TRPM8 outward currents at +100 mV during photoswitching at 23 °C and at 37 °C (Figure 3A). As expected, the activation and deactivation kinetics were significantly increased at 37 °C compared to 23 °C (Figure 3B and 3 C). τ_H for the deactivation ($\tau_H=73.2\pm15.4$ ms at 23 °C and $\tau_H=52.2\pm11.8$ ms at 37 °C) are more than 11-fold higher than for the activation ($\tau_H=6.6\pm1.6$ ms at 23 °C and $\tau_H=3.6\pm2.0$ ms at 37 °C). In addition, the inactivation kinetics were estimated by analyzing the time courses of the normalized outward currents during constant illumination with UV light of 365 nm (Figure 3D). The inactivation kinetics is biphasic comprising a fast followed by a slow inactivation phase ($\tau_{H1}=7.5\pm7.4$ s and $\tau_{H2}=193.4\pm56.1$ s at 23 °C; $\tau_{H1}=1.3\pm1.1$ s and $\tau_{H2}=90.9\pm29.2$ s at 37 °C) (Figure 3E).

Endogenously Expressed TRPM8 Channels can be Controlled by Light

To avoid animal experimentation, we tested different cell lines for endogenous TRPM8 expression. We found that the human prostate cancer cell line PC-3[31] functionally expresses TRPM8 channels that can be controlled by photoswitching (Figure 4). Whole-cell measurements with PC-3 cells in the presence of AzoM show that repeated photoswitching from blue light to UV light results in transient CD increases and decreases that can be blocked by the potent and selective TRPM8 blocker M8B. These findings suggest that AzoM is also suitable for light-induced activation of endogenously expressed TRPM8 channels.

Effects of AzoM on Potential AzoM Binding Mutants

Next, we aimed at shedding light upon the binding site of AzoM and investigating whether AzoM is useful for a comprehensive characterization of potential AzoM binding mutants.

3D structures in complex with (−)-menthol are still missing. Nevertheless, the binding sites for the cooling agents icilin,[32] WS-12,[32] C3[33] and AITC[33] were shown to be located in the voltage sensing like domain (VSLD) cavity of TRPM8 which is formed by the amino acids (numbers refer to human TRPM8; TM: transmembrane domain; TRPd: TRP domain; il2: intracellular linker between TM4 and TM5): $Y745^{TM1}$, $R842^{TM4}$, $H845^{TM4}$, $Y1005^{TRPd}$ and $R1008^{TRPd}$. The menthol-derivative WS-12 particularly binds to $Y745^{TM1}$, $R842^{TM4}$, $Y1005^{TRPd}$ and $R1008^{TRPd}$, and icilin to $Y745^{TM1}$, $R842^{TM4}$, $H845^{TM4}$ and $Y1005^{TRPd}$. The cooling agent C3 also binds to $Y745^{TM1}$, $R842^{TM4}$ and $H845^{TM4}$. The binding site of AITC differs from the icilin, WS-12 and C3 binding site and includes the amino acids $M801^{TM3}$, $W798^{TM3}$

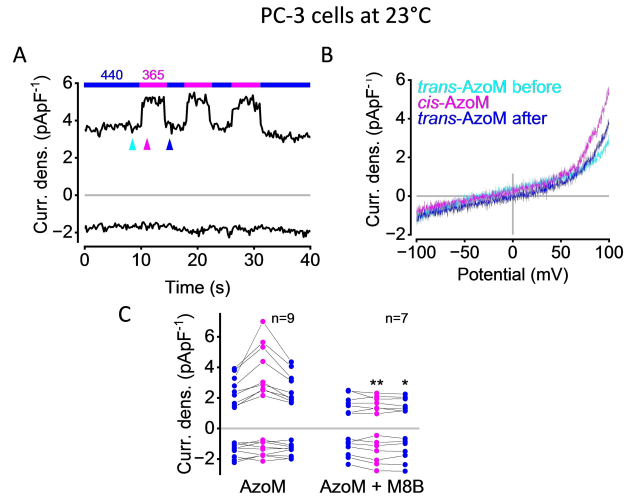

Figure 4. Endogenously expressed TRPM8 channels can be controlled by light. Whole-cell measurements of prostate cancer cells PC-3 that endogenously express TRPM8 channels in the presence of 50 µM AzoM measured at 23 °C. (A, B) Representative measurement with CD time course at ±100 mV (A) and corresponding CD voltage (CDV) relations in the presence of *trans*- and *cis*-AzoM (B) obtained by illumination using light of the wavelengths λ = 365 nm or λ = 440 nm. (C) Summaries of maximal CD ('Curr. dens.') at potentials of ±100 mV in the presence of *trans*-(blue dots) or *cis*-AzoM (violet dots) induced by photoswitching in the presence or absence of the selective TRPM8 blocker M8B (100 nM). Black asterisks indicate significances compared to *trans*- or *cis*-AzoM in the absence of M8B (**$P < 0.01$; *$P < 0.05$; Mann-Whitney U test).

and Q861^{il2}. Altogether, the binding sites for cooling agents surround the C-terminal part of TM4 and are located near the VSLD, the TRP domain and the pore domain.[32–33] Furthermore, mutagenesis approaches, summarized by Plaza-Cayon and colleagues,[34] suggested that (−)-menthol might interact with Y745^{TM1},[35] Q785^{TM2},[36] R842^{TM4},[37] and Y1005^{TRPd}.[35a] However, Yin and colleagues found that Q785^{TM2} interacts with a calcium ion in the same cavity[32] and therefore does not directly participate in agonist binding. Besides Q785^{TM2}, the amino acids E782^{TM2}, N799^{TM2} and D802^{TM3} also contribute to binding of calcium ions.[32] This calcium-binding site is located in the same cavity as the binding site for the cooling agents.

Based on these previous findings, we assumed that AzoM binds at a similar site as other cooling agents[32–33] in the VSLD cavity. To identify the potential binding site of *trans*- and *cis*-AzoM, we performed a molecular docking approach based on an open state model of TRPM8[38] using *trans*- and *cis*-AzoM compared to (−)-menthol, icilin, WS-12 and C3. The following amino acids emerged as potential binding sites for *trans*- and *cis*-AzoM and were exchanged by performing site-directed mutagenesis as indicated: N741A^{TM1}, Y745H^{TM1}, L778A^{TM2}, D781A^{TM2}, E782A^{TM2}, Q785A^{TM2}, N799A^{TM3}, D802A^{TM3}, G805A^{TM3}, F839A^{TM4}, R842A^{TM4}, L843A^{TM4}, I846V^{TM4}, and Y1005F^{TRPd} (Figure 5A and 5B).

All TRPM8 mutants were analyzed performing whole-cell measurements in the presence of 50 µM AzoM at room temperature to additionally monitor the effect of the amino acid exchanges on the cold-induced TRPM8 currents. Furthermore, the activation and deactivation kinetics were determined (Figure 5 and Supplemental Figure 4). Hereby, we proceed from the assumption that reduced *cis*-AzoM-induced CD amplitudes point to a participation in AzoM binding. In addition, we also assumed that slower activation and/or faster deactivation kinetics indicate a role in AzoM binding. The mutants N741A^{TM1} and L778A^{TM2} which occurred in the AzoM dockings, exhibited a complete impairment of channel function without any measurable current increases (Figure 5C and 5D). When calculating the NSC (Supplemental Figure 5), no differences between the NSC curves in the presence of *cis*- or *trans*-AzoM occurred, suggesting no channel activity. Consequently, no activation or deactivation kinetics could be determined.

While the *trans*-AzoM-induced CD of the mutant Y745H^{TM1} was similar to the wildtype CD, the *cis*-AzoM-induced CD was significantly reduced, pointing to a crucial role of Y745^{TM1} for AzoM binding which is corroborated by an about four-fold slower activation kinetics (Figure 5E). The mutant D781A^{TM2} also showed an impaired channel function with largely reduced CD, but with slight *cis*-AzoM-induced CD increases suggesting that the mutant D781A^{TM2} is still functional (Figure 5C and 5D). The deactivation kinetics were significantly faster compared to the wildtype channel (Figure 5F) pointing to a participation of D781^{TM2} in AzoM binding. The mutants E782A^{TM2}, Q785A^{TM2}, N799A^{TM3} and D802A^{TM3} which are involved in Ca^{2+} binding in the binding pocket, showed *cis*-AzoM-induced CD increases (Figure 5C and 5D). However, the mutants E782A^{TM2}, Q785A^{TM2}, and D802A^{TM3} exhibited overall reduced CD amplitudes, while the mutant N799A^{TM3} showed similar CD amplitudes as the wildtype channel. The mutants E782A^{TM2} and D802A^{TM3} showed faster deactivation (Figure 5F) and Q785A^{TM2} slower activation kinetics (Figure 5E). The mutant N799A^{TM3} showed even faster activation and deactivation kinetics (Figure 5E and 5F) suggesting that this amino acid is more likely to transduce agonist binding into channel gating, which is referred to as gating transduction, rather than contributing to agonist binding. Altogether, the calcium binding mutants that were previously suggested to stabilize the icilin binding,[32] define the 3D structure of the AzoM binding site thereby indirectly influencing the AzoM binding.

The mutant G805A^{TM3} also showed *cis*-AzoM-induced CD increases with overall reduced CD amplitudes (Figure 5C and 5D) and exhibited a significantly faster deactivation kinetics (Figure 5F) pointing to a direct contribution to AzoM binding. Calculating the NSC of the potential AzoM binding mutants, we found that all mutants except R842A^{TM4} exhibit different gating behavior compared to the wildtype channel (Supplemental Figures 6 and 7). The mutants F839A^{TM4} and R842A^{TM4} were both functional showing *cis*-AzoM induced CD increases with overall reduced CD amplitudes (Figure 5C and 5D). However, in case of F839A^{TM4}, the deactivation kinetics were slower (Figure 5F) opposing a direct participation in AzoM binding but rather implying a role for gating transduction.

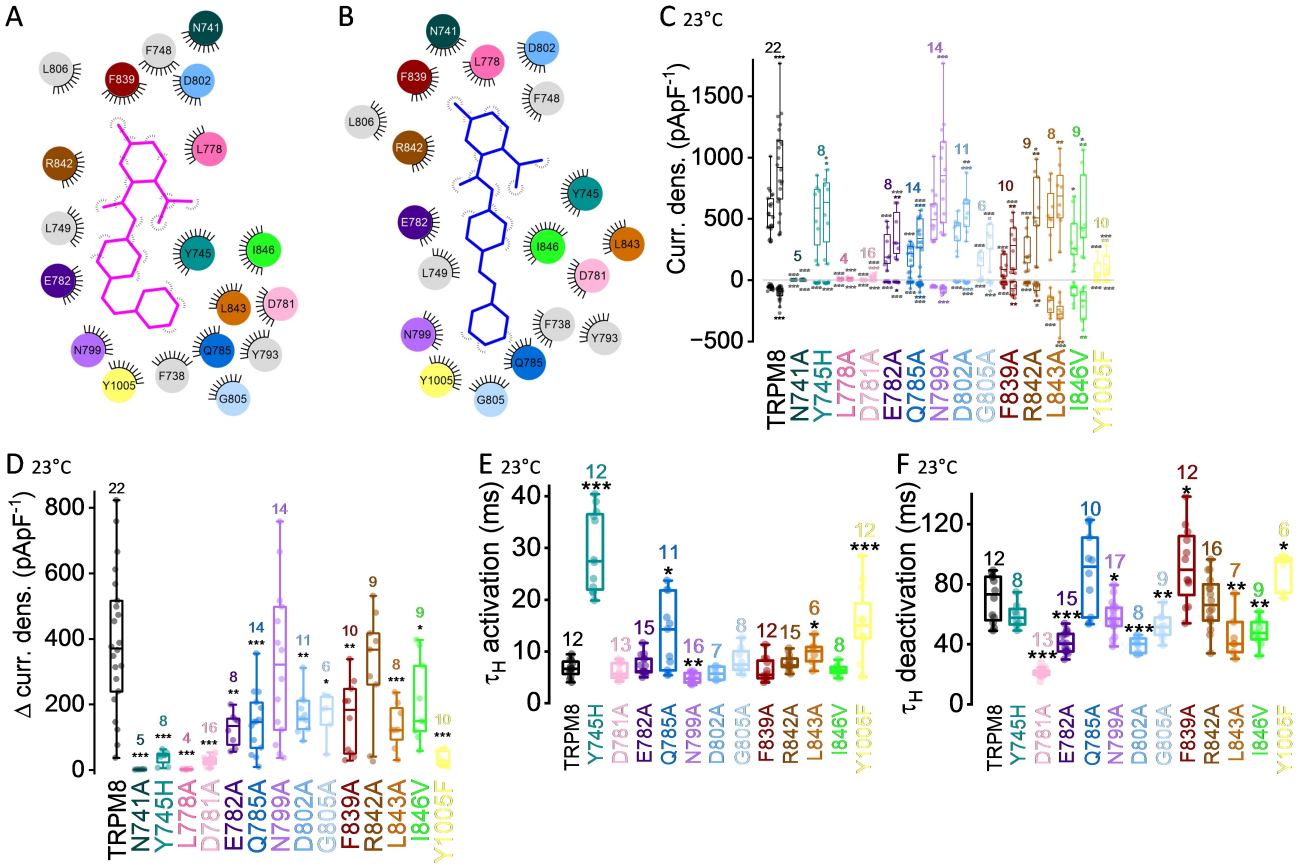

Figure 5. Effect of AzoM on potential AzoM binding mutants. (A, B) Synopsis of results from molecular docking approach with amino acids that are potentially involved in *trans*- and *cis*-AzoM binding. (C–F) Whole-cell measurements of HEK293T cells that overexpress TRPM8 or indicated TRPM8 mutants in the presence of 50 µM AzoM at 23 °C. (C) Summary of maximal CD ('Curr. dens.') at potentials of ±100 mV induced by *trans*-AzoM (left boxplot) or *cis*-AzoM (right boxplot). Black asterisks indicate significant differences compared to the wildtype (***$P<0.001$, **$P<0.01$; *$P<0.05$; Mann-Whitney U test), colored asterisks indicate significances between *trans*- and *cis*-AzoM (**$P<0.01$, ***$P<0.001$; *$P<0.05$; Wilcoxon matched-pairs signed-rank test). (D) Summary of normalized CD calculated as differences between *cis*- and *trans*-AzoM-induced CD. Asterisks indicate significant differences compared to wildtype (***$P<0.001$, **$P<0.01$; *$P<0.05$; Mann-Whitney U test). (E, F) Summaries of the half-time constants for activation ($\tau_{H\ activation}$) and for deactivation ($\tau_{H\ deactivation}$) at 23 °C. Asterisks indicate significance compared to wildtype (***$P<0.001$, **$P<0.01$; *$P<0.05$; Mann-Whitney U test). (C–F) Numbers over boxplots indicate numbers of measured cells. Data are displayed as boxplots and interquartile ranges. A fast up-ramp protocol with a frequency of 50 Hz was applied.

In contrast, in case of R842A^{TM4}, neither activation nor deactivation kinetics were changed (Figure 5E and 5F). The NSC curve progression of R842A^{TM4} was similar to that of wildtype TRPM8 (Supplemental Figure 7), suggesting that the amino acid exchange from arginine to alanine at position 842 reduces membrane expression, rather than influencing the channel gating. Because of the unchanged activation and deactivation kinetics, we assume no direct participation in AzoM binding. The mutant L843A^{TM4} showed largely increased inward CD amplitudes in the presence of *trans*-AzoM and decreased *cis*-AzoM induced outward CD (Figure 5C). Since L843A^{TM4} exhibited slower activation as well as faster deactivation kinetics (Figure 5E and 5F), this amino acid might directly participate in AzoM binding. The mutant I846V^{TM4} exhibited CD increases that were significantly smaller than the wildtype CD (Figure 5C and 5D) and a significantly faster deactivation kinetics (Figure 5F) suggesting that I842^{TM4} might directly contribute to AzoM binding. Furthermore, the mutant Y1005F^{TRPd} exhibited overall reduced CD amplitudes with only slight CD increases induced by *cis*-AzoM (Figure 5C and 5D) with slower activation and deactivation kinetics (Figure 5E and 5F) indicating that this amino acid is involved in gating transduction rather than in agonist binding.

To summarize, analysis of the current kinetics in combination with analysis of the CD amplitudes and the NSC are pointing to a participation of the amino acids Y745^{TM1}, D781^{TM2}, G805^{TM3}, L843^{TM4} and I846^{TM4} in AzoM binding. An overview of the suggested AzoM binding site is displayed in Supplemental Figure 8 (Videos). Altogether, AzoM allows for an extended biophysical analysis of TRPM8 currents encompassing not only the CD amplitudes but also the activation and deactivation current kinetics. Consulting the current kinetics was even possible when CD amplitudes or rather the membrane expression of the binding mutants were reduced. The determination of both parameters in combination with the NSC provides additional

insights into the function of amino acids and their role for gating transduction or agonist binding.

Influence of PIP_2 on the Kinetics of TRPM8 Currents

To assess the role of PIP_2 for current kinetics, we manipulated the intracellular PIP_2 levels by co-transfection of either an active phosphatidylinositol-4-phosphate 5-kinase ($PIP5K^{active}$) that increases PIP_2 levels or an inactive phosphatidylinositol-4-phosphate 5-kinase ($PIP5K^{inactive}$) that leaves endogenous PIP_2 levels unchanged. To diminish high cold-induced currents, the measurements were conducted at 37 °C. Photoswitching of AzoM causes significant CD increases at basal and increased PIP_2 levels (Figure 6A). In the absence of AzoM, no current increases were monitored (Figure 6A and 6B). *Trans*-AzoM and *cis*-AzoM-induced CD are significantly increased in the presence of $PIP5K^{active}$ suggesting that the $PIP5K^{active}$ is effective and enhances TRPM8 current amplitudes. When comparing the activation and inactivation kinetics of TRPM8 currents at basal and increased PIP_2 levels (Figure 6B and 6C), we found that higher PIP_2 levels tend to cause faster activation kinetics which are not significantly different. However, the deactivation kinetics are significantly slower in the presence of $PIP5K^{active}$ suggesting that increased PIP_2 levels do not only influence the current amplitudes but also the current kinetics.

Next, we analyzed the role of the potential PIP_2 binding mutants for TRPM8 channel gating. The binding site for PIP_2 was previously postulated to be situated within the TRP domain, a crucial structural feature of TRP channels. This binding site is comprised of the positively charged amino acids $K995^{TRPd}$, $R998^{TRPd}$ and $R1008^{TRPd}$.[39] However, recent advances in cryo-EM indicate that the PIP_2 binding site is in close proximity to the interfacial cavity of TRPM8 located between TM4, the TRP domain, and the pre-S1 domain. Notably, this site includes the previously postulated amino acid $R998^{TRPd}$.[32–33] However, the amino acids $R851^{il2}$ and $N852^{il2}$ which are located in the linker region between TM4 and TM5 also participate in PIP_2 binding.

We started with the potential PIP_2 binding mutants $K995A^{TRPd}$, $R998A^{TRPd}$ and $R1008A^{TRPd}$ which are located in the TRP domain and that were previously identified by mutational studies.[39] However, in contrast to Rohacs and colleagues[39] we replaced the positively charged amino acids with alanine. In addition, the amino acids $R851^{il2}$ and $N852^{il2}$ were also exchanged with alanine. In the presence of $PIP5K^{active}$, the *cis*- and *trans*-AzoM-induced CD of the mutants $R851A^{il2}$, $N852A^{il2}$, $R998A^{TRPd}$ and $R1008A^{TRPd}$ were very small when measured at 37 °C (Figure 6D). In contrast, the mutant $K995A^{TRPd}$ shows significantly increased *cis*- and *trans*-AzoM-induced CD at 37 °C pointing to a sensitization mutant. However, when performing whole-cell measurements of TRPM8 expressing HEK293T cells at room temperature and analyzing the cold-induced currents in the absence of AzoM, we found that all mutants are functional showing TRPM8 currents (Supplemental Figure 9). Analyzing the activation and deactivation kinetics of the mutants $R851A^{il2}$ and $N852A^{il2}$ in the presence of $PIP5K^{active}$ at 37 °C (Figure 6E and 6F), we found that both mutants show significantly slower activation and significantly faster deactivation kinetics, suggesting that the impaired PIP_2 binding influences the current kinetics. Unfortunately, the AzoM-induced currents of the mutants $R998A^{TRPd}$ and $R1008A^{TRPd}$ were too small to reliably analyze the current kinetics. Interestingly, the mutant $K995A^{TRPd}$ exhibits unchanged activation but significantly slower deactivation kinetics (Figure 6E and 6F), indicating that this mutant, although not directly involved in PIP_2 binding according to cryo-EM analysis,[32–33] enhances PIP_2 binding thereby diminishing the deactivation kinetics. Altogether, $K995A^{TRPd}$ emerged as a novel sensitization mutant that is more active when PIP_2 levels are increased, suggesting that this amino acid can foster PIP_2 binding by interacting with the adjacent amino acids $R851^{il2}$ and $N852^{il2}$ thereby stabilizing PIP_2 binding and improving sensitivity to AzoM. The localization of the analyzed amino acids is depicted in Figure 6G.

Discussion

In this study we demonstrate that the menthol-derivative AzoM serves as a high-precision pharmacological tool for optical control of TRPM8 channel activity in the heterologous expression system as well as in the endogenous expression system using prostate cancer cells PC-3[31] (Figure 2 and 4). *cis*-AzoM causes reliable and repeatable CD increases with an EC_{50} value of 4.4 ± 5.8 μM (Figure 2G) at 37 °C. However, *trans*-AzoM was also effective showing a concentration dependent inhibitory effect on cold-induced TRPM8 currents at room temperature (Figure 2I) with an IC_{50} of around 100 μM. These findings suggest that both AzoM isomers bind directly in the binding pocket of the channel, suggesting that the TRPM8 channel activation and deactivation kinetics are dependent on photoisomerization and independent of the diffusion of the compound into the binding pocket, since cells were pre-incubated with AzoM in our experimental setup.

The advantage of photoswitchable channel modulators lies within their capacity for precise temporal control of channel function and for localized, non-invasive modulation through the application of light of different wavelengths. This might be particularly interesting for the treatment of distinct areas of the body thereby avoiding systemic adverse drug reactions. Since TRPM8 channels turned out to be novel drug targets for the treatment of several diseases such as pain, migraine,[7] cold allodynia,[8] cancer,[9] dry eye disease,[10] irritable bowel syndrome, oropharyngeal dysphagia, chronic cough, hypertension[11a–e] as well as obesity and type 2 diabetes,[12] high-precision pharmaceuticals with reduced adverse drug reactions might be beneficial in the future.

AzoM was not only useful for precise control of TRPM8 channel activity, but also for determination of the TRPM8 activation, deactivation and inactivation kinetics (Figures 3, 5 and 6). This was not possible before because of wash-in and wash-out effects that usually occur, when channel

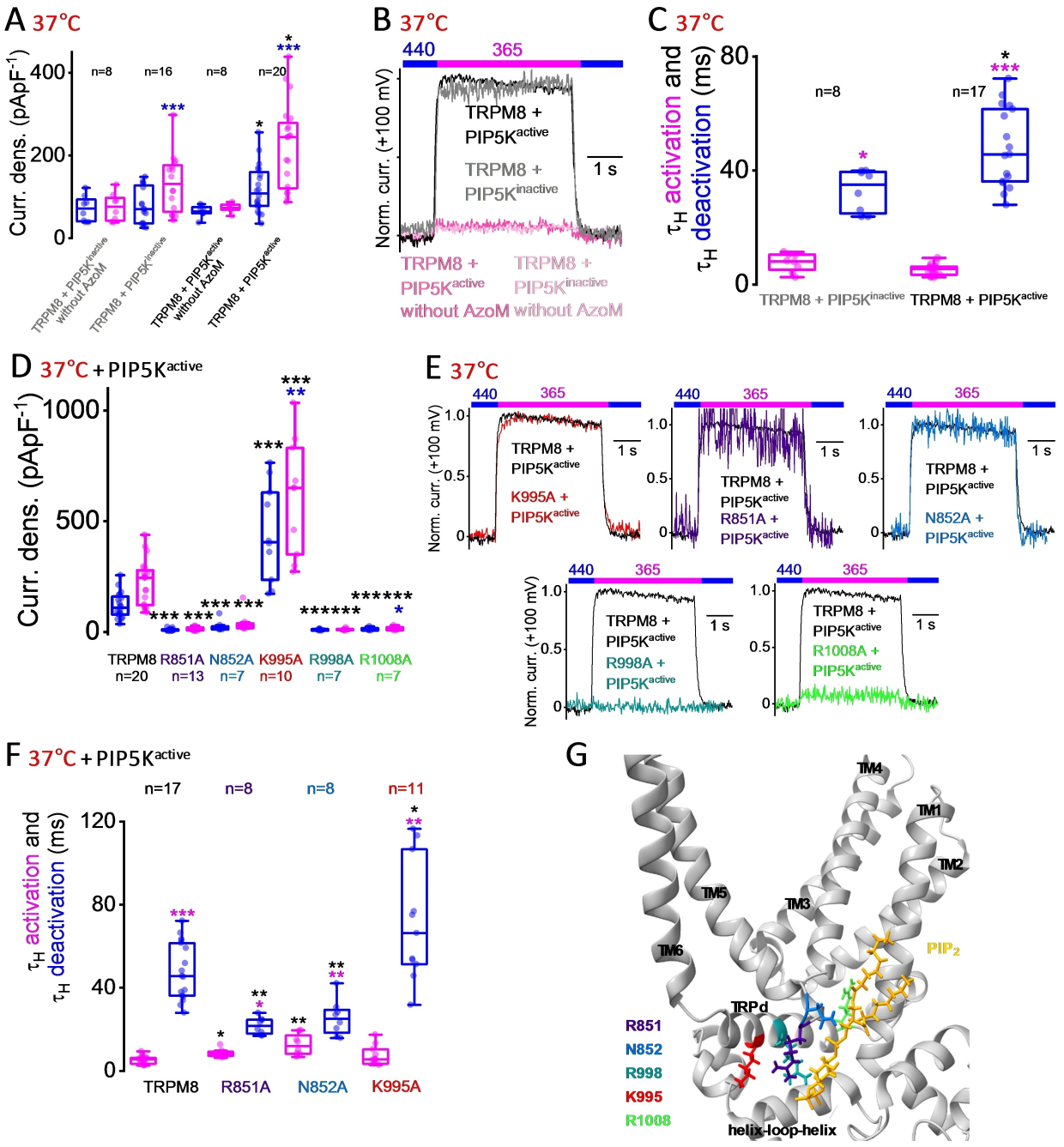

Figure 6. Influence of PIP_2 on the kinetics of TRPM8 currents. (A) Summary of maximal CD ('Curr. dens.') at +100 mV in the presence or absence of *trans*-(blue) or *cis*-AzoM (violet) of HEK293T cells that overexpress TRPM8 and an inactive ($PIP5K^{inactive}$) or active PIP5 K ($PIP5K^{active}$) to enhance intracellular PIP_2 levels. Black asterisks indicate significant differences compared to cells that express inactive PIP5 K (*$P<0.05$; Mann-Whitney U test), blue asterisks indicate significances between *trans*- and *cis*-AzoM (***$P<0.001$; Wilcoxon matched-pairs signed-rank test). (B) Representative time course of the normalized TRPM8 current induced by photoswitching in the presence of active and inactive PIP5 K and in the absence of AzoM. (C) Summary of the half-time constants for activation ($\tau_{H\ activation}$) (violet bars) and for deactivation ($\tau_{H\ deactivation}$) (blue bars) at 23 °C. Black asterisks indicate significance between cells that express active or inactive PIP5 K (*$P<0.05$; Mann-Whitney U test). Violet asterisks indicate significant difference between $\tau_{H\ activation}$ and $\tau_{H\ deactivation}$.(***$P<0.001$; *$P<0.05$; Wilcoxon matched-pairs signed-rank test). (D) Summary of maximal CD ('Curr. dens.') at +100 mV induced by *trans*-(blue) or *cis*-AzoM (violet) of HEK293T cells that overexpress TRPM8 or indicated TRPM8 mutants together with $PIP5K^{active}$. Black asterisks indicate significant differences compared to wildtype (***$P<0.001$; Mann-Whitney U test), blue asterisks indicate significances between *trans*- and *cis*-AzoM (*$P<0.05$; **$P<0.01$; ***$P<0.001$; Wilcoxon matched-pairs signed-rank test). (E) Representative time courses of the normalized currents of TRPM8 (black traces) and TRPM8 mutants (colored traces) induced by photoswitching in the presence of $PIP5K^{active}$. (F) Summary of the half-time constants for activation ($\tau_{H\ activation}$) (violet bars) and for deactivation ($\tau_{H\ deactivation}$) (blue bars) at 23 °C. Black asterisks indicate significance between cells that express $PIP5K^{active}$ (*$P<0.05$; Mann-Whitney U test). Violet asterisks indicate significant difference between $\tau_{H\ activation}$ and $\tau_{H\ deactivation}$.(**$P<0.01$; ***$P<0.001$; Wilcoxon matched-pairs signed-rank test). (A, C, D, F) Data are displayed as boxplots and interquartile ranges. A fast up-ramp protocol with a frequency of 50 Hz was applied. (G) 3D structure of TRPM8 based on PDB ID 8E4N with indicated amino acids and position of PIP_2.

activators are applied via the bath solution. Compared to the kinetics of OptoDArG-induced TRPC6 currents at 23 °C,[24] TRPM8 exhibited similar activation kinetics and 8.7-times slower deactivation kinetics, 40-times faster fast inactivation kinetics, and 14-times slower slow inactivation kinetics. AzoM-induced TRPM8 currents had deactivation kinetics more than 11-times slower than activation at both 23 °C and 37 °C. For TRPC6, deactivation was 1.4- to 2.5-times slower than activation with OptoDArG or OptoBI-1, respectively.[24] Both TRPM8 and TRPC6 exhibited biphasic inactivation, with TRPM8′s fast inactivation being 18.8- to 25-times slower and its slow inactivation 2.6- to 14.8-times slower than TRPC6.[24] These findings highlight photopharmacology's precision in distinguishing specific channel properties like current kinetics.

The use of AzoM enabled the measurement of temperature-induced increases in the activation, inactivation and deactivation kinetics (Figure 3) thereby demonstrating that AzoM is applicable for a valid and reliable determination of TRPM8 current kinetics based on the analysis of whole-cell currents.

Furthermore, when analyzing potential AzoM binding mutants, we found that using AzoM (Figure 5) does not only allow for determination of the maximal *trans*- and *cis*-AzoM-induced current densities which already provides information about the role of particular amino acids for AzoM-induced channel activation, but AzoM additionally provided detailed information about the activation and deactivation kinetics. Under the assumption that impaired AzoM binding manifests as either slower activation or faster deactivation kinetics or even both, we analyzed the potential AzoM binding mutants, accordingly. The following amino acids showed the respective changes in current kinetics and are thus presumably directly involved in AzoM binding: $Y745^{TM1}$, $D781^{TM2}$, $G805^{TM3}$, $L843^{TM4}$ and $I846^{TM4}$. The amino acid $Y745^{TM1}$ is well known as binding site for cooling agents such as icilin, C3, AITC and WS-12 and even menthol which was demonstrated in mutational studies.[32–33,35] Our results suggest that the amino acid $D781^{TM2}$ that emerged from AzoM and WS-12 docking is also involved in AzoM binding. The amino acid $G805^{TM3}$ was previously described as potential icilin but not as menthol binding mutant[3] and appeared in both icilin and AzoM dockings suggesting an overlap between the icilin and the AzoM binding site. Also, $L843^{TM4}$ and $I846^{TM4}$ that emerged from previous menthol dockings[38] as well as from current *cis*- and *trans*-AzoM dockings (Figure 5A and 5B), are likely to be directly involved in AzoM binding.

We initially used the open state model of *Ficedula albicollis* TRPM8 that exhibits an improved binding pocket structure for menthol.[38] This model was previously used to calculate conformational changes of TRPV1 channels.[40] Nevertheless, we performed additional molecular docking approaches with AzoM using the 3D structures of human[41] and mouse TRPM8[42] in the closed (ligand-free) state. In line with our earlier results, the amino acids Y745, D781 and I846 were found to be possibly involved in AzoM binding (Supplemental Figure 10). However, G805 and L843 did not occur in these dockings. Nevertheless, in principle the overlay of the three 3D structures in the presence of *trans*- or *cis*-AzoM suggests a similar binding site (Supplemental Figure 10B). By performing patch-clamp measurements and taking into account the current kinetics as well as the NSC, we obtained evidence that the five amino acids mentioned above might participate in AzoM binding. Molecular docking results should not be overrated since they depend on the quality of the available 3D structures and should be regarded as a first hint. Furthermore, ligand binding in the binding pocket leads to conformational changes that are not considered by conventional docking approaches. However, to verify our results, future cryo-EM analysis in the presence of AzoM is required.

When comparing our results to the predicted (−)-menthol binding site,[38] we can assume, that the isopropyl group of (−)-menthol adopts the same position in the binding pocket as that of AzoM. Therefore, van der Waals interactions between the "legs" of the isopropyl moiety with L843 and I838 are likely as demonstrated by Xu et al. 2020.[38] Van der Waals interactions are also achievable for Y745. However, the described hydrogen bond between R842 and the hydroxyl group of (−)-menthol is unlikely because AzoM lacks the hydroxyl group of (−)-menthol and instead possesses an amid moiety which is coupled to the azo-benzene moiety. Altogether, the AzoM binding site is located in the same cavity that serves for binding of other cooling agents such as icilin and menthol (Supplemental Figure 11; Video).

Our findings suggest that other amino acids might rather play a role for gating transduction than for agonist binding such as $N799^{TM3}$, $F839^{TM4}$ and $Y1005^{TRPd}$. Furthermore, the amino acids $E782^{TM2}$, $Q785^{TM2}$, $N799^{TM3}$ and $D802^{TM3}$ that are involved in Ca^{2+} binding in the agonist binding pocket[32] caused changes of the current kinetics although not directly involved in AzoM binding suggesting that these amino acids might define the 3D structure of the AzoM binding site thus indirectly influencing AzoM binding.

Furthermore, we found that the maximal *cis*-AzoM-, icilin- and (−)-menthol-induced CD voltage relations at 23 and 37 °C show distinct NSC curve progressions[43] suggesting different channel gating behaviors. These findings corroborate the idea that these cooling agents which have distinct binding properties in the VSDL domain of TRPM8 can cause distinct active channel states (Figure 2J). The NSC analysis was also useful to analyze the *trans*-AzoM-induced TRPM8 currents inhibition (Supplemental Figure 3) at 23 and 37 °C. We observed significant differences of the NSC curve progression mainly at outward currents that were most pronounced at 37 °C indicating that *trans*-AzoM causes a distinct inactive channel state with different gating behavior. In addition, NSC was helpful in analyzing binding mutants, revealing that reduced CD amplitudes, combined with unchanged current kinetics and NSC curve progressions, indicate normal channel gating but reduced membrane expression.

We observed, that increasing PIP_2 levels by coexpressing $PIP5K^{active}$ compared to endogenous PIP_2 levels cause increased TRPM8 CD (Figure 6A) which is corroborated by faster activation and slower deactivation kinetics (Fig-

ure 6C). Interestingly, we found that K995A^{TRPd} is a sensitization mutant which is in contrast to Rohacs and colleagues,[39] that described K995 as PIP_2 binding site and to Yin and colleagues,[32–33] who showed that K995 is not involved in PIP_2 binding. The amino acid R851^{il2} was described as PIP_2 binding site,[32] while N852^{il2} was only proposed as PIP_2 binding site.[33] We found that after amino acid exchanges to alanine the mutants R851A^{il2} and N852A^{il2} exhibit significantly reduced CD, slower activation and faster deactivation kinetics, which underlines the central role of these amino acids for PIP_2 binding. R851^{il2} and N852^{il2} are located in the linker region between TM4 and TM5 and the amino acid K995^{TRPd} which is located in the TRP domain laying directly behind R851 where it presumably influences PIP_2 binding. Since K995A^{TRPd} exhibits a sensitization phenotype with increased AzoM-induced CD and slower deactivation kinetics in the presence of high PIP_2 levels, this amino acid exchange presumably stabilizes and enhances the PIP_2 binding by allowing R851 and the adjacent amino acid N852 to slightly move (Figure 6G). Altogether, we identified a sensitizing mutant that increases PIP_2 binding which allows deeper insight into the binding and gating transduction of TRPM8 channels.

Conclusions

In conclusion, AzoM is a highly effective tool for advanced biophysical analysis of TRPM8 channels, offering precise spatio-temporal control over TRPM8 activity. It provides substantial advantages for the in-depth characterization of TRPM8 currents, particularly in its ability to detail current kinetics, which surpasses traditional measurements of current density and G/G_{max}. This, in turn, allows for a deeper understanding of the channel's gating behavior. Through photopharmacology, we demonstrate that photoswitchable channel activators not only offer precise regulation of channel function but also facilitate the identification of the specific roles individual amino acids play in gating and ligand binding.

Supporting Information

Supporting Information to experimental details, supplemental Figures and supporting videos related to Supplemental Figures 8 and 11 can be found in the Supporting Information section.

Authors Contributions

D. T. and D. B. K. initiated the study and supervised the chemical experiments. D. B. K. and K. L. designed, synthesized and analyzed the chemical properties of AzoM. M. MyS. and U. S. designed the biological experiments and supervised the study. J. B., C. S. E. and H. S. performed patch-clamp experiments. M. MyS., J. B., C. S. E., H. S. and C. H. analyzed the data. U. S., M. MyS. and D. B. K. wrote the manuscript. T. G. and D. T. revised the manuscript. C. H. prepared LED control and fit routine with MATLAB R2023a. M. MyS., J. B., C. S. E., H. S., C. H., U. S.and K. L. prepared the figures. All authors reviewed the manuscript.

Acknowledgements

We thank Laura Danner, Norbert Ertl, Michael Etterer und Jürgen Aust for excellent technical support and Thomas Voets for providing hTRPM8 cDNA and for hTRPM8 expressing HEK293 cell line. This work was supported by the German Research Foundation (Deutsche Forschungsgemeinschaft) project no. ME 2456/4-1 and TRR-152 project no. P26, by a Liebig fellowship from the Fonds der chemischen Industrie (FCI) and National Institutes of Health (Grant R01GM126228). Open Access funding enabled and organized by Projekt DEAL.

Conflict of Interest

The authors declare no conflict of interest.

Data Availability Statement

The data that support the findings of this study are available from the corresponding author upon reasonable request.

Keywords: photopharmacology · ion channels · TRPM8 · photoswitchable menthol · current kinetics

[1] G. Reid, M. L. Flonta, *Nature* **2001**, *413*, 480.
[2] a) D. D. McKemy, W. M. Neuhausser, D. Julius, *Nature* **2002**, *416*, 52–58; b) A. M. Peier, A. Moqrich, A. C. Hergarden, A. J. Reeve, D. A. Andersson, G. M. Story, T. J. Earley, I. Dragoni, P. McIntyre, S. Bevan, A. Patapoutian, *Cell* **2002**, *108*, 705–715.
[3] H. H. Chuang, W. M. Neuhausser, D. Julius, *Neuron* **2004**, *43*, 859–869.
[4] D. M. Bautista, J. Siemens, J. M. Glazer, P. R. Tsuruda, A. I. Basbaum, C. L. Stucky, S. E. Jordt, D. Julius, *Nature* **2007**, *448*, 204–208.
[5] S. Blanquart, A. S. Borowiec, P. Delcourt, M. Figeac, C. A. Emerling, A. S. Meseguer, M. Roudbaraki, N. Prevarskaya, G. Bidaux, *Mol. Phylogenet. Evol.* **2019**, *136*, 104–118.
[6] R. Paricio-Montesinos, F. Schwaller, A. Udhayachandran, F. Rau, J. Walcher, R. Evangelista, J. Vriens, T. Voets, J. F. A. Poulet, G. R. Lewin, *Neuron* **2020**, *106*, 830–841 e833.
[7] N. R. Gavva, R. Sandrock, G. E. Arnold, M. Davis, E. Lamas, C. Lindvay, C. M. Li, B. Smith, M. Backonja, K. Gabriel, G. Vargas, *Sci. Rep.* **2019**, *9*, 19655.
[8] a) L. Su, C. Wang, Y. H. Yu, Y. Y. Ren, K. L. Xie, G. L. Wang, *BMC Neurosci.* **2011**, *12*, 120; b) C. J. Proudfoot, E. M. Garry, D. F. Cottrell, R. Rosie, H. Anderson, D. C. Robertson, S. M. Fleetwood-Walker, R. Mitchell, *Curr. Biol.* **2006**, *16*, 1591–1605.
[9] A. Hantute-Ghesquier, A. Haustrate, N. Prevarskaya, V. Lehen′kyi, *Pharmaceuticals (Basel)* **2018**, *11*.
[10] J. M. Yang, E. T. Wei, S. J. Kim, K. C. Yoon, *Pharmaceuticals (Basel)* **2018**, *11*.

[11] a) M. Iftinca, C. Altier, *Channels (Austin)* **2020**, *14*, 413–420; b) F. Huang, M. Ni, J. M. Zhang, D. J. Li, F. M. Shen, *Molecular medicine reports* **2017**, *15*, 1900–1908; c) M. Henstrom, F. Hadizadeh, A. Beyder, F. Bonfiglio, T. Zheng, G. Assadi, J. Rafter, L. Bujanda, L. Agreus, A. Andreasson, A. Dlugosz, G. Lindberg, P. T. Schmidt, P. Karling, B. Ohlsson, N. J. Talley, M. Simren, S. Walter, M. Wouters, G. Farrugia, M. D'Amato, *Gut* **2017**, *66*, 1725–1727; d) S. J. Bonvini, M. G. Belvisi, *Pulm. Pharmacol. Ther.* **2017**, *47*, 21–28; e) D. Alvarez-Berdugo, L. Rofes, J. F. Casamitjana, A. Enrique, J. Chamizo, C. Vina, C. M. Pollan, P. Clave, *Neurogastroenterol Motil* **2018**, *30*, e13398; f) P. Uvin, J. Franken, S. Pinto, R. Rietjens, L. Grammet, Y. Deruyver, Y. A. Alpizar, K. Talavera, R. Vennekens, W. Everaerts, D. De Ridder, T. Voets, *Eur. Urol.* **2015**, *68*, 655–661.

[12] C. Clemmensen, S. Jall, M. Kleinert, C. Quarta, T. Gruber, J. Reber, S. Sachs, K. Fischer, A. Feuchtinger, A. Karlas, S. E. Simonds, G. Grandl, D. Loher, E. Sanchez-Quant, S. Keipert, M. Jastroch, S. M. Hofmann, E. B. M. Nascimento, P. Schrauwen, V. Ntziachristos, M. A. Cowley, B. Finan, T. D. Muller, M. H. Tschop, *Nat. Commun.* **2018**, *9*, 4304.

[13] B. Beck, G. Bidaux, A. Bavencoffe, L. Lemonnier, S. Thebault, Y. Shuba, G. Barrit, R. Skryma, N. Prevarskaya, *Cell Calcium* **2007**, *41*, 285–294.

[14] J. M. Yang, F. Li, Q. Liu, M. Ruedi, E. T. Wei, M. Lentsman, H. S. Lee, W. Choi, S. J. Kim, K. C. Yoon, *BMC Ophthalmol.* **2017**, *17*, 101.

[15] A. Janssens, M. Gees, B. I. Toth, D. Ghosh, M. Mulier, R. Vennekens, J. Vriens, K. Talavera, T. Voets, *eLife* **2016**, *5*.

[16] E. Zakharian, C. Cao, T. Rohacs, *J. Neurosci.* **2010**, *30*, 12526–12534.

[17] B. M. Vickerman, E. M. Zywot, T. K. Tarrant, D. S. Lawrence, *Nat Rev Chem* **2021**, *5*, 816–834.

[18] a) J. A. Frank, D. A. Yushchenko, D. J. Hodson, N. Lipstein, J. Nagpal, G. A. Rutter, J. S. Rhee, A. Gottschalk, N. Brose, C. Schultz, D. Trauner, *Nat. Chem. Biol.* **2016**, *12*, 755–762; b) T. Leinders-Zufall, U. Storch, K. Bleymehl, M. Mederos y Schnitzler, J. A. Frank, D. B. Konrad, D. Trauner, T. Gudermann, F. Zufall, *Cell Chem. Biol.* **2018**, *25*, 215–223 e213; c) T. Leinders-Zufall, U. Storch, M. Mederos y Schnitzler, N. K. Ojha, K. Koike, T. Gudermann, F. Zufall, *STAR Protoc* **2021**, *2*, 100527.

[19] M. Lichtenegger, O. Tiapko, B. Svobodova, T. Stockner, T. N. Glasnov, W. Schreibmayer, D. Platzer, G. G. de la Cruz, S. Krenn, R. Schober, N. Shrestha, R. Schindl, C. Romanin, K. Groschner, *Nat. Chem. Biol.* **2018**, *14*, 396–404.

[20] O. Tiapko, N. Shrestha, S. Lindinger, G. Guedes de la Cruz, A. Graziani, C. Klec, C. Butorac, W. F. Graier, H. Kubista, M. Freichel, L. Birnbaumer, C. Romanin, T. Glasnov, K. Groschner, *Chem. Sci.* **2019**, *10*, 2837–2842.

[21] a) J. A. Frank, M. Moroni, R. Moshourab, M. Sumser, G. R. Lewin, D. Trauner, *Nat. Commun.* **2015**, *6*, 7118; b) D. B. Konrad, J. A. Frank, D. Trauner, *Chemistry* **2016**, *22*, 4364–4368.

[22] M. Müller, K. Niemeyer, N. Urban, N. K. Ojha, F. Zufall, T. Leinders-Zufall, M. Schaefer, O. Thorn-Seshold, *Angew. Chem. Int. Ed.* **2022**, *61*, e202201565.

[23] P. Y. Lam, A. R. Thawani, E. Balderas, A. J. P. White, D. Chaudhuri, M. J. Fuchter, R. T. Peterson, *J. Am. Chem. Soc.* **2020**, *142*, 17457–17468.

[24] M. Keck, C. Hermann, K. Lützel, T. Gudermann, D. B. Konrad, M. Mederos y Schnitzler, U. Storch, *iScience* **2024**, *27*, 111008.

[25] M. Schoenberger, A. Damijonaitis, Z. Zhang, D. Nagel, D. Trauner, *ACS Chem. Neurosci.* **2014**, *5*, 514–518.

[26] M. A. Sherkheli, A. K. Vogt-Eisele, D. Bura, L. R. Beltran Marques, G. Gisselmann, H. Hatt, *J. Pharm. Pharm. Sci.* **2010**, *13*, 242–253.

[27] D. A. Andersson, H. W. Chase, S. Bevan, *J. Neurosci.* **2004**, *24*, 5364–5369.

[28] a) D. Cunningham, E. T. Gallagher, D. H. Grayson, P. J. McArdle, C. B. Storey, D. J. Wilcock, *J. Chem. Soc. Perkin Trans. 1* **2002**, 2692–2698; b) P. A. Senaratne, F. M. Orihuela, A. J. Malcolm, K. G. Anderson, *Org. Process Res. Dev.* **2003**, *7*, 185–186.

[29] E. Fischer, *J. Phys. Chem.* **1967**, *71*, 3704–3706.

[30] S. Brauchi, P. Orio, R. Latorre, *Proc. Natl. Acad. Sci. USA* **2004**, *101*, 15494–15499.

[31] S. Asuthkar, L. Demirkhanyan, X. Sun, P. A. Elustondo, V. Krishnan, P. Baskaran, K. K. Velpula, B. Thyagarajan, E. V. Pavlov, E. Zakharian, *J. Biol. Chem.* **2015**, *290*, 2670–2688.

[32] Y. Yin, S. C. Le, A. L. Hsu, M. J. Borgnia, H. Yang, S. Y. Lee, *Science* **2019**, *363*.

[33] Y. Yin, F. Zhang, S. Feng, K. J. Butay, M. J. Borgnia, W. Im, S. Y. Lee, *Science* **2022**, *378*, eadd1268.

[34] A. Plaza-Cayon, R. Gonzalez-Muniz, M. Martin-Martinez, *Med. Res. Rev.* **2022**, *42*, 2168–2203.

[35] a) M. Bandell, A. E. Dubin, M. J. Petrus, A. Orth, J. Mathur, S. W. Hwang, A. Patapoutian, *Nat. Neurosci.* **2006**, *9*, 493–500; b) A. Malkia, M. Pertusa, G. Fernandez-Ballester, A. Ferrer-Montiel, F. Viana, *Mol. Pain* **2009**, *5*, 62.

[36] M. M. Diver, Y. Cheng, D. Julius, *Science* **2019**, *365*, 1434–1440.

[37] T. Voets, G. Owsianik, A. Janssens, K. Talavera, B. Nilius, *Nat. Chem. Biol.* **2007**, *3*, 174–182.

[38] L. Xu, Y. Han, X. Chen, A. Aierken, H. Wen, W. Zheng, H. Wang, X. Lu, Z. Zhao, C. Ma, P. Liang, W. Yang, S. Yang, F. Yang, *Nat. Commun.* **2020**, *11*, 3790.

[39] T. Rohacs, C. M. Lopes, I. Michailidis, D. E. Logothetis, *Nat. Neurosci.* **2005**, *8*, 626–634.

[40] F. Yang, X. Xiao, B. H. Lee, S. Vu, W. Yang, V. Yarov-Yarovoy, J. Zheng, *Nat. Commun.* **2018**, *9*, 2879.

[41] S. Palchevskyi, M. Czarnocki-Cieciura, G. Vistoli, S. Gervasoni, E. Nowak, A. R. Beccari, M. Nowotny, C. Talarico, *Commun. Biol.* **2023**, *6*, 1065.

[42] Y. Yin, C. G. Park, F. Zhang, G. F. J, S. Feng, Y. Suo, W. Im, S. Y. Lee, *Sci. Adv.* **2024**, *10*, eadp2211.

[43] C. Hermann, A. Treder, M. Naher, R. Geiseler, T. Gudermann, M. Mederos y Schnitzler, U. Storch, *Biophys. J.* **2022**, *121*, 1435–1448.

Manuscript received: September 2, 2024
Accepted manuscript online: December 11, 2024
Version of record online: ■■, ■■

Research Article

Ion Channels

J. Becker, C. S. Ellerkmann, H. Schmelzer, C. Hermann, K. Lützel, T. Gudermann, D. B. Konrad,* D. Trauner,* U. Storch,* M. Mederos y Schnitzler* — **e202416549**

Optical Control of TRPM8 Channels with Photoswitchable Menthol

We developed azo-menthol (AzoM), the first photoswitchable activator of the TRPM8 channel. AzoM enables precise and reversible optical control of TRPM8, facilitating detailed analysis of current kinetics. This allows for deeper insights into the specific roles of individual amino acids in channel gating, AzoM binding, and phosphoinositol-4,5-bisphosphate (PIP_2) binding and sensitization.